pubs.acs.org/Biomac

Article

Single Enzyme Nanoparticles with Improved Biocatalytic Activity through Protein Entrapment in a Surfactant Shell

Dylan L. Atkins, J. Rodrigo Magana, Christian C. M. Sproncken, Jan C.M. van Hest, and Ilja K. Voets*

Cite This: *Biomacromolecules* 2021, 22, 1159–1166

Read Online

ACCESS | Metrics & More | Article Recommendations | Supporting Information

ABSTRACT: A polymeric corona consisting of an alkyl-glycolic acid ethoxylate (C_XEO_Y) surfactant offers a promising approach toward endowing proteins with thermotropic phase behavior and hyperthermal activity. Typically, preparation of protein−surfactant biohybrids is performed *via* chemical modification of acidic residues followed by electrostatic conjugation of an anionic surfactant to encapsulate single proteins. While this procedure has been applied to a broad range of proteins, modification of acidic residues may be detrimental to function for specific enzymes. Herein, we report on the one-pot preparation of biohybrids *via* covalent conjugation of surfactants to accessible lysine residues. We entrap the model enzyme hen egg-white lysozyme (HEWL) in a shell of carboxyl-functionalized $C_{12}EO_{10}$ or $C_{12}EO_{22}$ surfactants. With fewer surfactants, our covalent biohybrids display similar thermotropic phase behavior to their electrostatically conjugated analogues. Through a combination of small-angle X-ray scattering and circular dichroism spectroscopy, we find that both classes of biohybrids consist of a folded single-protein core decorated by surfactants. Whilst traditional biohybrids retain densely packed surfactant coronas, our biohybrids display a less dense and heterogeneously distributed surfactant coverage located opposite to the catalytic cleft of HEWL. In solution, this surfactant coating permits 7- or 3.5-fold improvements in activity retention for biohybrids containing $C_{12}EO_{10}$ or $C_{12}EO_{22}$, respectively. The reported alternative pathway for biohybrid preparation offers a new horizon to expand upon the library of proteins for which functional biohybrid materials can be prepared. We also expect that an improved understanding of the distribution of tethered surfactants in the corona will be crucial for future structure−function investigations.

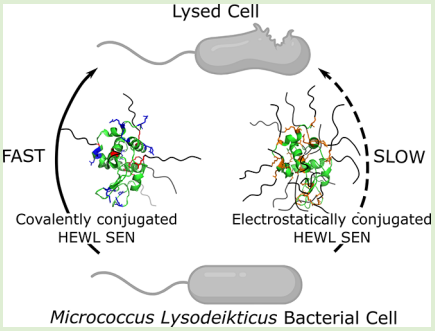

INTRODUCTION

Enzymes are exploited in many personal care products, foods, therapeutics, and industrial processes due to their evolutionary honed specificity and efficiency.[1−5] A recurrent complication in their application is their poor chemical and structural stability in non-native environments.[2−4] Furthermore, preparation and long-term storage of high-concentration protein-based formulations are challenging due to the high propensity for aggregation.[1,6] Encapsulating enzymes into polymeric nanocarriers generally provides protection toward harsh non-native conditions, protease digestion, and temperature, among others. Advantageously, chemical modifications in the protective shell afford additional functionalities to the enzyme, such as targeted delivery and responsiveness to external stimuli.[7] The preparation of conventional protein capsules is commonly performed by statistically trapping enzymes into polymeric nanoparticles, vesicles, or inorganic surfaces.[8] Despite the advantages provided by these (in)organic armors, they only allow for the diffusion of relatively small substrates, which may drastically reduce enzymatic performance toward large substrates. For example, multiple egg-white lysozyme (HEWL) embedded in a complex coacervate core micelle display enhanced activity toward small substrates compared to free HEWL; however, it is unfit to lyse cells.[9,10] This hindrance can be overcome by reducing the thickness and density of the encapsulating matrix, for example, by surface-tethering (short) polymers or growing thin polymer shells around single enzymes to generate single enzyme nanoparticles (SENs).[11]

Recently, amphiphiles with a block alkyl-glycolic acid ethoxylate (alkyl-EO) architecture have emerged as exciting targets for the discrete nanoencapsulation of single enzymes.[12−14] This is owed to their nature to self-assemble, which offers a means to stabilize proteins in new environments. For example, in the total absence of a solvent, protein−surfactant nanoconjugates display thermotropic behavior and hyperthermal stability.[15−17] A surfactant corona also facilitates stabilization in a range of solvents such as organic solvents and ionic liquids.[13,18,19] The multistep preparation of electrostatically assembled SENs from enzymes and surfactants generally consists of chemical modification of solvent-accessible acidic residues (cationic supercharging of Asp/Glu) followed by electrostatic conjugation of anionic surfactant to coat the

Received: November 24, 2020
Revised: February 5, 2021
Published: February 25, 2021

https://dx.doi.org/10.1021/acs.biomac.0c01663
Biomacromolecules 2021, 22, 1159−1166

protein surface. This approach aims to maximize the number of possible conjugation sites to achieve high-density coverage on the protein surface. Numerous reports evidence that various enzymes can be modified in this manner with limited loss of enzymatic activity. However, this route is not generally applicable to more fragile enzymes due to the harsh chemical conditions used during supercharging. In addition, modification of the acidic residues on the catalytic cleft may lead to enzymatic deactivation. To mitigate such challenges, Zhang et al. prepared SENs *via* layer-by-layer assembly of oppositely charged surfactants on the protein surface.[20] This appealing strategy improved enzymatic activity; however, stability may be insufficient at elevated ionic strengths when electrostatic interactions are weakened.

Aiming to develop a versatile, alternative pathway to prepare single enzyme nanoparticles (SENs) encapsulated with surfactants, we set out to explore if such biohybrids could be prepared through a straightforward, one-pot covalent conjugation of surfactant molecules to lysine residues. We selected the model enzyme, HEWL, for our purposes because it is inaccessible to large cellular substrates when encapsulated within polymeric nanocarriers but may be accessible within SENs. In addition, the catalytic cleft of HEWL contains acidic residues that make HEWL incompatible with previously reported procedures.[21,22] To this end, the solvent-accessible Lys residues of HEWL were coupled to the EDC activated carboxyl-termini of the alkyl-glycolic acid ethoxylate surfactants $C_{12}EO_{10}$ or $C_{12}EO_{22}$. Targeting Lys residues led to a surface coverage of up to ∼17 surfactants per enzyme with an anisotropic distribution and opposite to the HEWL catalytic pocket, in sharp contrast to the 26 surfactants that were homogeneously distributed on the supercharged HEWL. Remarkably, the covalent hybrids still displayed thermotropic behavior in the solvent-free state whilst retaining up to >90% activity in solution toward large cellular substrates, which is 3.5-fold higher activity than their electrostatic analogues.

EXPERIMENTAL METHODS

Biohybrid Preparation. All materials were purchased from Sigma-Aldrich (NL) and used without further purification. Hen egg-white lysozyme (HEWL, lot # 117K1547) was suspended in phosphate buffer (10 mM PB, pH 6.5) to achieve a final concentration of 2 mg ml^{-1}. The number of potential anchoring sites was obtained from the crystal structure of HEWL (DOI: 10.2210/pdb1DPX/pdb).

For covalently conjugated biohybrids, the surfactants glycolic acid ethoxylate lauryl ether ($C_{12}EO_{10}$), or carboxylated[14] Brij L23 ($C_{12}EO_{22}$) were dissolved in buffer to achieve a final concentration of 20 mg mL^{-1}. To activate the carboxylic acid, solid *N*-(3-dimethylaminopropyl)-*N*′-ethylcarbodiimide hydrochloride (EDC, 104 μmol) was mixed with the surfactant solution (34 μmol) and was allowed to stir for 30 min. The protein solution (8.6 μmol) was subsequently added to achieve a 4-fold molar excess of surfactant with respect to solvent-accessible Lys residues. The reaction mixture was allowed to stir overnight followed by removal of any precipitate by centrifugation (4000*g*, 15 min) and extensive dialysis using 10 kDa MWCO cellulose tubes against decreasing concentrations of buffer into a final dialysis against MilliQ quality water in a time frame of 72 h.

For electrostatically conjugated biohybrids, 3-(dimethylamino)-1-propylamine (DMAPA, 2.2 M and pH 6.2) was added to at least 500-fold molar excess (40 mmol) to the number of solvent-accessible acidic side chains of HEWL (3.47 μmol, estimated from the HEWL crystalline structure) followed by the immediate addition of solid EDC in a further 10-fold excess (800 μmol). After 4 h, a secondary addition of EDC (800 μmol) was performed, and the reaction was allowed to proceed overnight to produce a supercharged enzyme. Any precipitate was removed by centrifugation (4000*g*, 15 min) followed by extensive dialysis against buffer. The supercharged enzyme was added dropwise under stirring to neat $C_{12}EO_{10}$ or $C_{12}EO_{22}$ dissolved in minimum buffer containing an excess of four surfactants per cationic site and allowed to stir overnight. High-order aggregates were removed by centrifugation, and the protein solution was dialyzed as the covalent SENs above.

All purified biohybrids were freeze-dried for 48 h to produce a soft solid powder and thermally annealed at 80 °C to produce a free-flowing liquid. Biohybrids were then stored in a desiccator under vacuum and at room temperature. All aqueous characterization of the SENs was performed in samples previously annealed at 80 °C.

Differential Scanning Calorimetry. Differential scanning calorimetry experiments were performed on a TA Instruments Q2000. Samples were first incubated at 80 °C to remove thermal history and cooled at 10 °C min^{-1} to −60 °C. Thermal cycles were subsequently performed between −60 °C to +80 °C at a constant temperature gradient of 10 °C min^{-1}. At least two cycles were performed to ensure that sample phase behavior was unchanged and material degradation did not occur.

X-ray Scattering Data Acquisition. The experiments were performed on a SAXSLAB GANESHA 300 XL system equipped with a GeniX-Cu source (λ = 1.54 Å, flux of 1×10^8 Ph s^{-1}) and a Pilatus 300 K silicon pixel detector. The scattering intensity was measured as a function of momentum transfer vector

$$q = \frac{4\pi}{\lambda} \sin\theta \tag{1}$$

where 2θ is the scattering angle. The 2D patterns from the detector were azimuthally averaged to generate 1D scattering profiles. SEN solutions were measured in 2.0 mm quartz capillaries (Hilgenberg), mounted with custom-built capillary holders in a q-range of $0.015 < q < 0.445$ $Å^{-1}$. Data treatment was performed using a SAXSutilities[23] package (http://www.sztucki.de/SAXSutilities). All profiles are obtained from merging at least two scattering profiles collected at different (high/low) concentrations in 10 mM phosphate buffer (pH 6.5). The SAXS profiles were further analyzed to determine the number of enzymes per hybrid, the grafting density of surfactants, and the radius of gyration (R_g).

Guinier Analysis. SAXS profiles were further analyzed to determine the number of enzymes per hybrid, the grafting density of surfactants, and the radius of gyration (R_g). To this end, the molecular weights of biohybrid variants (M_{SAXS}) were computed from the forward scattering intensity extrapolated to zero q (I_0), which was extracted from a Guinier analysis of the SAXS profiles. Guinier plots ($\ln[I(q)]$ vs q^2) were produced for the scattering profiles, from which I_0 (cm^{-1}) and R_g (Å) were determined using

$$I(q) \approx I_0 e^{-(q^2 R_g^2)/3} \tag{2}$$

from the region of the profile, satisfying the condition $qR_g < 1.3$ for globular proteins.[24,25] Next, M_{SAXS} was computed from the forward intensity values, I_0:

$$M_{SAXS} = I_0 \frac{N_{av}}{C\Delta\rho_M^2} \tag{3}$$

where N_{av} is Avogadro's number (6.023×10^{23} mol^{-1}), C is the construct concentration, and $\Delta\rho_M$ (cm g^{-1}) is the scattering contrast per mass computed using

$$\Delta\rho_M = [\rho_{M,prot} - (\rho_{solv}\bar{\nu})]r_0 \tag{4}$$

where $\rho_{M,prot}$ is the number of electrons per mass of dry protein (3.22×10^{23} e g^{-1}), ρ_{solv} is the number of electrons per volume of solvent (3.34×10^{23} e cm^{-3}), $\bar{\nu}$ is the partial specific volume of protein (0.7425 cm^3 g^{-1}), and r_0 is the scattering length of an electron (2.8179×10^{-13} cm).

https://dx.doi.org/10.1021/acs.biomac.0c01663
Biomacromolecules 2021, 22, 1159−1166

Scheme 1. Schematic Representation of Protein−Surfactant SENs Prepared *via* (a) Electrostatic Surfactant Tethering and (b) Covalent Surfactant Binding[a]

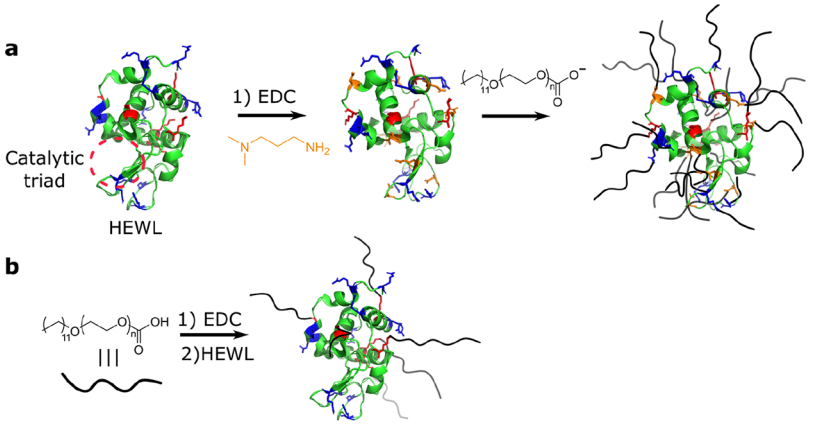

[a]The residues to which the surfactants are anchored are color coded in red (lysine), blue (arginine), and orange (cationized aspartamic and glutamic acid). The HEWL catalytic triad is also highlighted in red.

As the total number of surfactants tethered per protein is unknown and, consequently, the concentration of construct is also not known, we performed self-consistent computations until the following expression converged to unity:

$$\frac{M_{SAXS}}{M_{SEN}} = I_0 \frac{N_{av}}{c_{HEWL} \times M_{SEN} \times \Delta\rho_M^2} \times \frac{1}{M_{SEN}} \quad (5)$$

where c_{HEWL} is the protein concentration in mM obtained from UV−vis experiments and M_{SEN} is the molecular weight of the SENs defined as

$$M_{SEN} = M_{HEWL} + N_{surf} \times M_{surf} \quad (6)$$

where M_{HEWL}, M_{surf}, and N_{surf} are the molecular weight of HEWL, molecular weight of the surfactant used, and the number of surfactants attached to the construct.

Finally, the purity, p%, of the construct was calculated as

$$p\% = \frac{M_{SAXS} \times c_{HEWL}}{C_T} \times 100 \quad (7)$$

where C_T is the total concentration of product in solution in g/cm^3.

Circular Dichroism Spectroscopy. Circular dichroism spectroscopy measurements were executed on a Jasco J-815 between 260 and 190 nm at a scanning speed of 20 nm min^{-1}, with 4 s accumulation, 1 nm bandwidth, and a data pitch of 0.5 nm. All samples were measured using a 0.1 cm quartz cuvette. Protein concentrations were adjusted to maximize signal-to-noise ratios and by ensuring that HT values remained below 650 V. Each CD trace is obtained from averaging at least three measurements followed by background subtraction. Data is plotted using a three-point moving average. To elucidate the details of structural reorganization, we performed secondary structure deconvolution using the online Dichroweb server using the CDSSTR algorithm and associated reference set 4.[26,27] All outputs satisfied the condition of NRMSD < 0.025.

Kinetics Assays Using Cellular Substrates. All experiments were performed on a Tecan Safire^2 UV−vis plate reader with a standard sample path length of 0.81 cm (300 μL volume), and the temperature was controlled at 25 °C. The HEWL-mediated lysis of *Micrococcus lysodeikticus* (MLys) bacterial whole-cell walls was followed by the decrease in absorbance (increase in transmission) at 450 nm (A_{450}) over time, which was conducted for up to 600 s. Experiments were performed in buffer (10 mM PB, pH 6.5) with a constant [HEWL] of 0.5 μM and [MLys] of 0.15 mg mL^{-1}. Lysis activities were determined from the slope of the linear region of the absorbance change with time (maintained at 180 s for all assays), where 1 U mg^{-1} is defined as a ΔA_{450} of 0.001 per 60 s and mass of HEWL component. All data presented is the average of experiments performed in triplicate, with error bars indicating the standard deviation. Retained lysis activity of biohybrids is represented as a percentage of activity compared with native HEWL.

RESULTS AND DISCUSSION

Synthesis of Covalent and Noncovalent Protein−Surfactant Hybrids. Protein−surfactant SENs are generally prepared through a multistep procedure involving chemical supercharging followed by electrostatic conjugation of an oppositely charged surfactant to the supercharged protein surface (Scheme 1a).[12−17,28] As the surfactant shell is attached to the protein in a noncovalent manner, it may be released when electrostatic interactions are weakened. On the one hand, this reversibility may be useful if the enzyme is to be released, e.g., if the shell blocks access to the active site. On the other hand, it renders the encapsulation and concomitant stabilization pH- and salt-dependent. Furthermore, protein supercharging is not generally applicable to all enzymes since it aggressively modifies all the accessible acidic residues.

Aiming to expand the repertoire of preparation methods for surfactant-based SENs, we developed an alternative route to prepare stable biohybrids involving the covalent attachment of surfactant molecules to the surface accessible lysine residues on the protein (Scheme 1b). We illustrate the opportunities of this technology by a direct comparison of the properties in solvent-free and solution-state of electrostatic and covalent biohybrids of hen egg-white lysozyme (HEWL) and alkyl-glycolic acid ethoxylate block surfactants ($C_{12}EO_{10}$ or $C_{12}EO_{22}$). The covalently conjugated biohybrids were prepared in a straightforward, one-pot approach by EDC-mediated coupling of a carboxyl-terminated surfactant to solvent-accessible lysine (Lys) residues on the HEWL surface (see Experimental Methods). Briefly, the carboxyl-terminated surfactant was reacted with EDC to produce an activated ester intermediate. The addition of protein initiated the coupling with the solvent-accessible primary amines on the HEWL surface, yielding either HEWL-$C_{12}EO_{10}$ or HEWL-$C_{12}EO_{22}$. The analogous noncovalent biohybrids were prepared *via* the well-established route of supercharging followed by electrostatic coupling (see Experimental Methods).[14,15,17] Briefly, this first involved the covalent modification of solvent-accessible acidic residues (Asp/Glu) *via* EDC-mediated coupling of 1,3-dimethylamino propylamine (DMAPA) to produce a cationic

https://dx.doi.org/10.1021/acs.biomac.0c01663
Biomacromolecules 2021, 22, 1159−1166

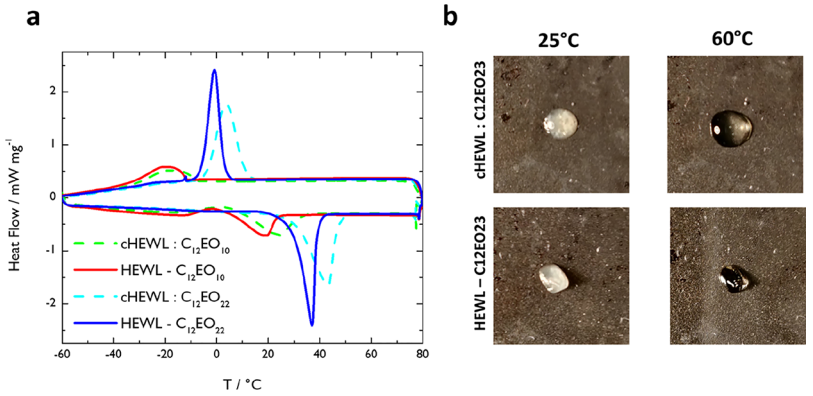

Figure 1. (a) Differential scanning calorimetry (DSC) traces comparing reversible melting and recrystallization transitions of covalently conjugated and electrostatically conjugated biohybrid variants in the absence of solvent. Comparison of cHEWL:$C_{12}EO_{10}$ (green dashed line) and HEWL-$C_{12}EO_{10}$ (red solid line) or cHEWL:$C_{12}EO_{22}$ (cyan dashed line) and HEWL-$C_{12}EO_{22}$ (blue solid line). Reduced melting and recrystallization temperatures are observed for covalently conjugated ($T_{HEWL\text{-}C12EO10}$ = 19 °C; $T_{HEWL\text{-}C12EO22}$ = 36 °C) biohybrids compared with their charge-stabilized counterparts ($T_{cHEWL:C12EO10}$ = 25 °C; $T_{cHEWL:C12EO22}$ = 43 °C). (b) Representative images of cHEWL:$C_{12}EO_{22}$ and HEWL-$C_{12}EO_{22}$ before (25 °C) and after (60 °C) melting.

Table 1. Biohybrid Molecular Weights Calculated Using the Guinier Analysis of Solution-State Small-Angle X-ray Scattering (SAXS) Experiments (M_{SAXS})

parameter	HEWL	HEWL-$C_{12}EO_{10}$	HEWL-$C_{12}EO_{22}$	cHEWL:$C_{12}EO_{10}$	cHEWL:$C_{12}EO_{22}$
purity (%)		68.5	62.4	85.1	80.6
M_{SAXS} (kDa)	14.0	29.3	38.0	36.4	48.6
R_g (Å)	14.5	35.1	30.6	37.2	37.5
# surfactants		23.2	19.4	34.2	28.2

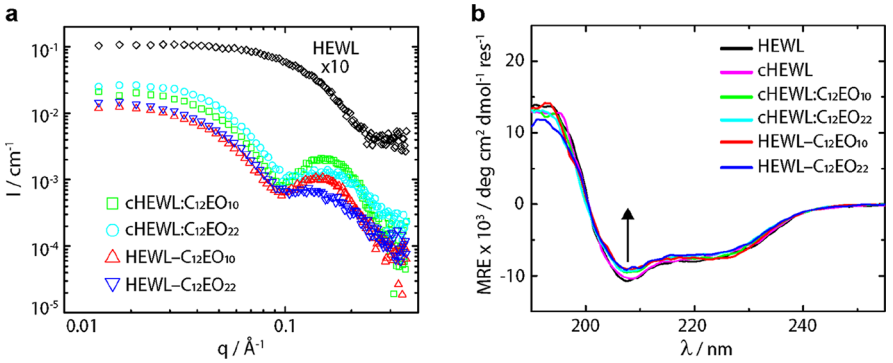

Figure 2. (a) SAXS profiles of native HEWL (×10, black diamonds), cHEWL:$C_{12}EO_{10}$ (green squares), cHEWL:$C_{12}EO_{22}$ (cyan circles), HEWL-$C_{12}EO_{10}$ (red upward triangles), and HEWL-$C_{12}EO_{22}$ (blue downward triangles). Scattering profiles indicate distinct structural transformations from a native protein to biohybrids consisting of single protein−polymer core−shell architectures, and forward q scattering intensities are used to compute the molecular weight (M_{SAXS}) of the nanoconjugates. (b) CD spectroscopy profiles after annealing the SENs in the absence of solvent of aqueous solutions of native HEWL (black), cHEWL (pink), cHEWL:$C_{12}EO_{10}$ (green), cHEWL:$C_{12}EO_{22}$ (cyan), HEWL-$C_{12}EO_{10}$ (red), and HEWL-$C_{12}EO_{22}$ (blue). CD traces show high degrees of secondary structure retention upon protein cationization followed by small losses of native folds upon conjugation with surfactants.

supercharged variant (cHEWL). We estimated that roughly five of nine solvent-accessible Asp/Glu residues were modified using matrix-assisted laser desorption/ionization time-of-flight (MALDI-TOF) mass spectrometry, which corresponds to a coupling efficiency of approximately 56%. We subsequently prepared electrostatically conjugated biohybrids by mixing of cHEWL with anionic surfactants, yielding cHEWL:$C_{12}EO_{10}$ and cHEWL:$C_{12}EO_{22}$.

The number of potential sites (i.e., six Lys) for covalent coupling to HEWL is considerably lower than the number of solvent-accessible cationic residues on cHEWL (5 reacted Asp/Glu residues + 6 Lys + 11 Arg). In addition, the anionic surfactants can also electrostatically anchor to positively charged arginines (11 Arg). The biohybrids also differ notably in the distribution of surfactants on the enzyme surface. The surfactant shell of the covalent hybrid is anisotropic as the solvent-accessible lysine residues on the HEWL surface are all roughly located in one hemisphere of the protein surface. By contrast, after supercharging, the positively charged residues are homogeneously distributed over the surface of cHEWL and possibly inside the catalytic triad (Figure S1). Therefore, we anticipate a more isotropic distribution of surfactant across the cHEWL surface.

Melting Behavior of Solvent-Free Surfactant-Based Covalent SENs. To assess if one of the most singular properties of surfactant-based SENs, the solvent-free protein

https://dx.doi.org/10.1021/acs.biomac.0c01663
Biomacromolecules 2021, 22, 1159−1166

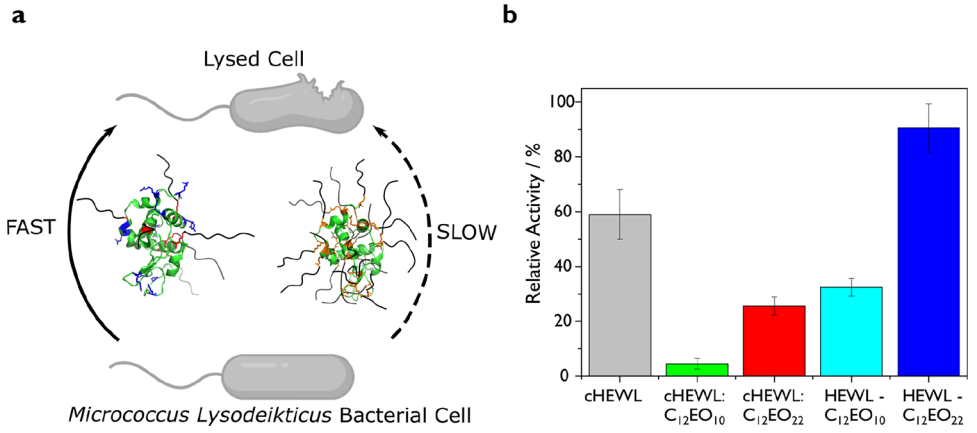

Figure 3. (a) Schematic representation of the HEWL-mediated lysis of *M. lysodeikticus* bacterial substrates for the covalently conjugated (left) or electrostatically conjugated (right) biohybrid variants. (b) Retained activity of protein−surfactant biohybrids estimated from lysis assays (represented as % compared to native HEWL). Relative activities indicate that covalently coupled biohybrids retain significantly greater activity than their charge-stabilized counterparts.

liquid state, was still present in the covalent variants, we performed differential scanning calorimetry (DSC) (Figure 1a). Remarkably, the HEWL-$C_{12}EO_{10}$ and HEWL-$C_{12}EO_{22}$ SENs melted with fewer surfactants per enzyme, just like their electrostatic counterparts (Figure 1b). Both covalent variants display melting and recrystallization phase transitions at lower temperatures than their isotropic counterparts. The reduction in melting and recrystallization transitions is attributed to the diminished conformational freedom of the surfactants being covalently attached to the protein surface. This reduction in degree of freedom causes the surfactant−surfactant interactions to be weakened, therefore making it easier to transit into a liquid phase. It is worth noticing that UV−vis determination of the total protein content on the SEN solutions revealed up to 40% excess unbound surfactant for all the products (Table 1). This may affect the melting temperatures. To determine whether this melting behavior was a result of excess surfactant or from the SEN formation, we prepared freeze-dried mixtures of surfactant and HEWL with the same ratio as those present in the SENS. Remarkably, these do not melt, not even at higher temperatures (Figure S2).

Solution-State Structure and Morphology. After annealing and melting the solvent-free SENs at 80 °C, these were redispersed in aqueous buffer. To elucidate the solution-state structure and morphology of the prepared biohybrid variants, we performed small-angle X-ray scattering (SAXS) experiments (Figure 2a). To determine how many surfactants are bound to the enzyme, we first determined biohybrid molecular weights from Guinier analysis (M_{SAXS}) on the SAXS data (Table 1, see the Experimental Methods).[25,29] Excess surfactant was accounted for in the calculation of M_{SAXS}; however, the computed M_{SAXS} might still be overestimated due to the presence of surfactant micelles with a higher molecular weight than monomerically dissolved surfactants. It is also worth noting that the forward scattering intensity of the corresponding SAXS patterns was slightly reduced due to a small yet noticeable influence of the structure factor at small q-values, which was not considered in the analysis. This effect may also lead to a slight error in the determined molecular weights. The obtained values for M_{SAXS} and the number of anchored surfactants were consistently smaller for the covalently conjugated biohybrids than for their electrostatically conjugated counterparts. As expected, M_{SAXS} values of biohybrids containing the shorter $C_{12}EO_{10}$ surfactant were smaller than those with $C_{12}EO_{22}$. Remarkably, M_{SAXS} and the number of anchored surfactants (22 and 17 for electrostatic and covalent constructs, respectively) exceeded the number of covalent and electrostatic anchoring sites. We tentatively attribute this to the above discussed overestimation of M_{SAXS} due to micellization of excess unbound surfactant. As expected, we also observed an increase in R_g upon conjugation of surfactant to produce the covalent and supramolecular conjugate. The SAXS results thus demonstrate the successful construction of SENs containing one protein decorated by a (non)covalently attached shell of surfactants. Attempts to measure the mass spectra of the biohybrids were not successful due to the presence of anionic surfactants in the matrix, which suppressed the signal.[30]

Irrespective of the conjugation approach, the SAXS profiles of the hybrid particles were distinctly different from the SAXS profiles of the native protein counterparts and characteristic for a core−shell architecture consisting of a single protein decorated by a surfactant corona.[14,31,32] The positions of the first interference minima are slightly displaced to higher q-values compared to those in the profiles of the $C_{12}EO_{22}$ micelles (Figure S3). This shift indicates that the hydrophobic tails of the surfactant corona are collapsed over the surface of HEWL, rendering a smaller core radius for the hybrid particles than for the surfactant micelles. The width and intensity of the shell contribution to the scattering profiles are more smeared in the SAXS profiles of the covalent SENs. This difference is attributed to the inhomogeneous coverage of the surfactant molecules on the surface of the covalent hybrids, which raises the so-called "blob scattering" contributions at high q-values due to the non-centrosymmetric nature of the particles.[33] Furthermore, we observed a reduced shell intensity for the $C_{12}EO_{22}$ hybrids with a longer EO block than the $C_{12}EO_{10}$ hybrids. We tentatively attribute this effect to a greater degree of hydration and concomitantly reduced electron density for the more hydrophilic surfactant with the larger EO block.

Having established the successful nanoencapsulation of individual proteins within a surfactant corona for both the supramolecular and covalent PEGylation routes, we set out to probe the degree of structural preservation of the globular protein core by circular dichroism (CD) spectroscopy (Figure 2b). For all HEWL-based biohybrids, we observed the minimal

https://dx.doi.org/10.1021/acs.biomac.0c01663
Biomacromolecules 2021, 22, 1159−1166

Table 2. Catalytic Performance of Native HEWL and Respective Protein−Surfactant Biohybrid Variants

parameter	HEWL	cHEWL	cHEWL:$C_{12}EO_{10}$	HEWL-$C_{12}EO_{10}$	cHEWL:$C_{12}EO_{22}$	HEWL-$C_{12}EO_{22}$
activity (U mg^{-1})	19,285	11,461	875	4935	6249	17,469
St Dev (U mg^{-1})	1650	1230	366	315	476	791
activity retained (%)		59.1 ± 8.3	4.5 ± 1.9	32.4 ± 1.6	25.6 ± 2.5	90.6 ± 4.1

influence of surfactant on the protein secondary structure but noted a small loss in the total energy of folding, given the reduced intensity of the CD traces. This is consistent with a previous report for electrostatically conjugated HEWL biohybrids.[24] This was further supported through secondary structure deconvolution using the online Dichroweb server (Table S1 and Figure S3).[26,27] As expected, no appreciable structural reorganization for HEWL-based biohybrids was detected. It is noteworthy that these samples were previously heated and incubated at 80 °C in the solvent-free state for 1 h, which highlights the hyperthermal stability of these biohybrids and could be used for protein storage at room temperature.

Enhanced Activity Afforded by an Anisotropic Corona. Encouraged by the high degree of secondary structure retention displayed by all HEWL biohybrids, we turned to quantitative measurements of enzymatic activity. Kinetic assays were performed by UV−vis spectroscopy using intact, micrometer-sized cells of *M. lysodeikticus* as a substrate (Figure 3a). Herein, cell wall lysis was monitored as a decrease in optical density recorded at a fixed wavelength of 450 nm (A_{450}). Based upon the initial linear decrease in A_{450} (Figure S4), we computed an activity of 19,285 ± 1650 U mg^{-1} for the native HEWL (Table 2). As expected from PEGylation procedures described in literature,[34,35] both surface functionalization strategies lead to some enzymatic deactivation. For covalently conjugated biohybrids, we determined activities of 6249 ± 476 U mg^{-1} (HEWL-$C_{12}EO_{10}$) and 17,469 ± 791 U mg^{-1} (HEWL-$C_{12}EO_{22}$), corresponding to 32.4 ± 1.6% and 90.6 ± 4.1% remnant activities, respectively (Figure 3b). This suggests that access to the catalytic cleft is restricted, albeit not prohibitively for this large substrate. By contrast, for the electrostatically conjugated biohybrids cHEWL:$C_{12}EO_{10}$ and cHEWL:$C_{12}EO_{22}$, we determined activities of 875 ± 366 U mg^{-1} and 4935 ± 315 U mg^{-1}, respectively. These retained merely 4.5 ± 1.9% and 25.6 ± 2.5% of the activity of native HEWL. Hence, the covalent SENs display an impressive 7- and 3.5-fold enhancement in solution-state activity compared to the supramolecular SENs.

The results of the kinetic assays may be rationalized by HEWL deactivation upon cationization into cHEWL, a surfactant blocking the activity cleft and/or structural differences in the surfactant corona. Chemical deactivation may be due to DMAPA-modification of Glu35 and/or Asp52, which are in the HEWL catalytic cleft and hence crucial for lysis activity.[21,22,36] However, we find that the cationized lysozyme retains ∼60% activity and is thus more active than the resulting complexes. This suggests that the acidic groups on the HEWL catalytic triad are not (completely) modified and that the surfactant shell hampers access of the substrate to the active site. In contrast, the covalent SENs may also retain higher activity because the covalent modification is performed on the opposite side of the catalytic cleft, facilitating the accessibility of cell substrates to the active site compared to the electrostatically assembled SENs. The lower numbers of surfactants in the covalent SENs compared to the electrostatic analogues may also promote access of bulky substrates to the catalytic cleft. This is in line with findings for PEGylated lysozyme, which displays lower activity retention for larger amounts of tethered PEO chains.[34]

Interestingly and opposed to PEGylation, in which higher molecular weights of PEO lead to lower activity retention,[34] SENs prepared with $C_{12}EO_{10}$ were less active than the biohybrids containing $C_{12}EO_{22}$. In view of the nearly congruent CD spectra, this difference appears unrelated to the structure of the encapsulated HEWL. We attribute this effect to a preference of the HEWL SENs to remain close to the cellular membrane and in consequence to the substrate. The longer PEO block may allow the alkyl chains to interdigitate better between phospholipids as compared to the shorter ones. A similar result was observed for other protein−surfactant complexes in which the amphiphilic corona afforded better integration of the complex within the cellular phospholipid membrane.[37] Moreover, the greater hydrophilicity of $C_{12}EO_{22}$ with the more than 2-fold longer PEO block may result in a higher affinity for the hydrophilic peptidoglycans on the bacterial surface.

CONCLUSIONS

In conclusion, we have prepared a new class of protein−surfactant SENs through direct covalent conjugation of surfactants to the surface of individual proteins. The impact of the one-step synthesis route on the HEWL structure and the properties of the resultant SENs was explored by CD, SAXS, and kinetic assays of HEWL activity. The same experiments were performed for biohybrids produced *via* a two-step approach of cationic supercharging followed by electrostatically mediated surfactant conjugation to quantitatively compare the structure and properties of the two types of SENs. Crucially, we show that liquefaction of proteins can still be achieved with fewer surfactants tethered to the protein surface. Overall, our covalently conjugated biohybrids displayed thermotropic behavior and advantageously lower temperature phase transitions. Solution-state structural investigations revealed that single HEWL−surfactant nanoconjugates with a core−shell architecture could be produced with the surfactants $C_{12}EO_{10}$ and $C_{12}EO_{22}$. CD spectra revealed little influence on the globular structure of the protein core. Surprisingly, this facilitated the retention of 90% lysis activity for the nanoconjugate HEWL-$C_{12}EO_{22}$ against large bacterial substrates. This amounted to a significant activity enhancement (up to 7-fold) compared to the electrostatically conjugated counterpart. The retention of enzymatic activity is attributed to the anisotropic polymer coverage opposite to the catalytic cleft and the circumvention of the modification of one or several essential catalytic residues in HEWL. We envisage that our preparation approach will significantly improve the use of SENs in applications requiring a narrow pH or ionic strength as the covalent conjugation renders higher chemical stability toward these conditions. Moreover, by targeting different amino acid residues, this preparation route expands the preparation of functional surfactant-based SENs to a broader variety of enzymes.

https://dx.doi.org/10.1021/acs.biomac.0c01663
Biomacromolecules 2021, 22, 1159−1166

■ ASSOCIATED CONTENT

Supporting Information

The Supporting Information is available free of charge at https://pubs.acs.org/doi/10.1021/acs.biomac.0c01663.

Continuum electrostatic calculations for HEWL; thermal bulk behavior of a mixture of surfactant and protein; SAXS comparison between surfactant micelles and SENs; secondary structure deconvolution analysis from circular dichroism spectroscopy traces; and HEWL kinetic assays using bacterial substrates (PDF)

■ AUTHOR INFORMATION

Corresponding Author

Ilja K. Voets − *Laboratory of Self-Organizing Soft Matter, Department of Chemical Engineering and Chemistry and Institute for Complex Molecular Systems, Department of Chemical Engineering and Chemistry, Eindhoven University of Technology, 5600 MB Eindhoven, The Netherlands;* orcid.org/0000-0003-3543-4821; Email: i.voets@tue.nl

Authors

Dylan L. Atkins − *Laboratory of Self-Organizing Soft Matter, Department of Chemical Engineering and Chemistry and Institute for Complex Molecular Systems, Department of Chemical Engineering and Chemistry, Eindhoven University of Technology, 5600 MB Eindhoven, The Netherlands;* orcid.org/0000-0003-1618-2059

J. Rodrigo Magana − *Laboratory of Self-Organizing Soft Matter, Department of Chemical Engineering and Chemistry and Institute for Complex Molecular Systems, Department of Chemical Engineering and Chemistry, Eindhoven University of Technology, 5600 MB Eindhoven, The Netherlands;* orcid.org/0000-0001-8637-1467

Christian C. M. Sproncken − *Laboratory of Self-Organizing Soft Matter, Department of Chemical Engineering and Chemistry and Institute for Complex Molecular Systems, Department of Chemical Engineering and Chemistry, Eindhoven University of Technology, 5600 MB Eindhoven, The Netherlands;* orcid.org/0000-0001-5303-0519

Jan C.M. van Hest − *Institute for Complex Molecular Systems, Department of Chemical Engineering and Chemistry, Eindhoven University of Technology, 5600 MB Eindhoven, The Netherlands; Laboratory of Bio-Organic Chemistry, Department of Chemical Engineering and Chemistry, Eindhoven University of Technology, 5600 MB Eindhoven, The Netherlands;* orcid.org/0000-0001-7973-2404

Complete contact information is available at: https://pubs.acs.org/10.1021/acs.biomac.0c01663

Notes

The authors declare no competing financial interest.

■ ACKNOWLEDGMENTS

This work was financially supported by the European Union (ERC-2014-StG Contract No. 635928) and Dutch Ministry of Education, Culture and Science (Gravity Program 024.001.035).

■ REFERENCES

(1) Shire, S. J.; Shahrokh, Z.; Liu, J. Challenges in the Development of High Protein Concentration Formulations. *J. Pharm. Sci.* **2004**, *93*, 1390−1402.

(2) Wang, W. Instability, Stabilization, and Formulation of Liquid Protein Pharmaceuticals. *Int. J. Pharm.* **1999**, *185*, 129−188.

(3) Polizzi, K. M.; Bommarius, A. S.; Broering, J. M.; Chaparro-Riggers, J. F. Stability of Biocatalysts. *Curr. Opin. Chem. Biol.* **2007**, *11*, 220−225.

(4) Jemli, S.; Ayadi-Zouari, D.; Hlima, H. B.; Bejar, S. Biocatalysts: Application and Engineering for Industrial Purposes. *Crit. Rev. Biotechnol.* **2014**, *36*, 246−258.

(5) Silva, C.; Martins, M.; Jing, S.; Fu, J.; Cavaco-Paulo, A. Practical Insights on Enzyme Stabilization. *Crit. Rev. Biotechnol.* **2018**, *38*, 335−350.

(6) Frokjaer, S.; Otzen, D. E. Protein Drug Stability: A Formulation Challenge. *Nat. Rev. Drug Discov.* **2005**, *4*, 298−306.

(7) Magana, J. R.; Sproncken, C. C. M.; Voets, I. K. On Complex Coacervate Core Micelles: Structure-Function Perspectives. *Polymers (Basel).* **2020**, *12*, 1953.

(8) Balcão, V. M.; Vila, M. M. D. C. Structural and Functional Stabilization of Protein Entities: State-of-the-Art. *Adv. Drug Delivery Rev.* **2015**, *93*, 25−41.

(9) Lindhoud, S.; De Vries, R.; Schweins, R.; Cohen Stuart, M. A.; Norde, W. Salt-Induced Release of Lipase from Polyelectrolyte Complex Micelles. *Soft Matter* **2009**, *5*, 242−250.

(10) Harada, A.; Kataoka, K. On-off Control of Enzymatic Activity Synchronizing With Reversible Formation of Supramolecular Assembly from Enzyme and Charged Block Copolymers. *J. Am. Chem. Soc.* **1999**, *121*, 9241−9242.

(11) Chapman, R.; Stenzel, M. H. All Wrapped up: Stabilization of Enzymes within Single Enzyme Nanoparticles. *J. Am. Chem. Soc.* **2019**, *141*, 2754−2769.

(12) Brogan, A. P. S.; Sharma, K. P.; Perriman, A. W.; Mann, S. Enzyme Activity in Liquid Lipase Melts as a Step towards Solvent-Free Biology at 150 °c. *Nat. Commun.* **2014**, *5*, 5058.

(13) Brogan, A. P. S.; Bui-Le, L.; Hallett, J. P. Non-Aqueous Homogenous Biocatalytic Conversion of Polysaccharides in Ionic Liquids Using Chemically Modified Glucosidase. *Nat. Chem.* **2018**, *10*, 859−865.

(14) Atkins, D. L.; Berrocal, J. A.; Mason, A. F.; Voets, I. K. Tandem Catalysis in Multicomponent Solvent-Free Biofluids. *Nanoscale* **2019**, *11*, 19797−19805.

(15) Perriman, A. W.; Cölfen, H.; Hughes, R. W.; Barrie, C. L.; Mann, S. Solvent-Free Protein Liquids and Liquid Crystals. *Angew. Chem., Int. Ed.* **2009**, *48*, 6242−6246.

(16) Brogan, A. P. S.; Siligardi, G.; Hussain, R.; Perriman, A. W.; Mann, S. Hyper-Thermal Stability and Unprecedented Re-Folding of Solvent-Free Liquid Myoglobin. *Chem. Sci.* **2012**, *3*, 1839.

(17) Perriman, A. W.; Brogan, A. P. S.; Cölfen, H.; Tsoureas, N.; Owen, G. R.; Mann, S. Reversible Dioxygen Binding in Solvent-Free Liquid Myoglobin. *Nat. Chem.* **2010**, *2*, 622−626.

(18) Zhang, Y.; Patil, A. J.; Perriman, A. W.; Mann, S. Enhanced Catalytic Activity in Organic Solvents Using Molecularly Dispersed Haemoglobin-Polymer Surfactant Constructs. *Chem. Commun.* **2013**, *49*, 9561−9563.

(19) Brogan, A. P. S.; Hallett, J. P. Solubilizing and Stabilizing Proteins in Anhydrous Ionic Liquids through Formation of Protein−Polymer Surfactant Nanoconstructs. *J. Am. Chem. Soc.* **2016**, *138*, 4494−4501.

(20) Zhang, W. H.; Carter, B. M.; Day, G. J.; Govan, N.; Jackson, C.; Perriman, A. W. Sequential Electrostatic Assembly of a Polymer Surfactant Corona Increases Activity of the Phosphotriesterase ArPTE. *Bioconjugate Chem.* **2019**, *30*, 2771−2776.

(21) Matsumura, I.; Kirsch, J. F. Is Aspartate 52 Essential for Catalysis by Chicken Egg White Lysozyme? The Role of Natural Substrate-Assisted Hydrolysis. *Biochemistry* **1996**, *35*, 1881−1889.

(22) Hashimoto, Y.; Yamada, K.; Motoshima, H.; Omura, T.; Yamada, H.; Yasukochi, T.; Miki, T.; Ueda, T.; Imoto, T. A Mutation Study of Catalytic Residue Asp 52 in Hen Egg Lysozyme. *J. Biochem.* **1996**, *119*, 145−150.

(23) Sztucki, M.; Narayanan, T. Development of an Ultra-Small-Angle X-Ray Scattering Instrument for Probing the Microstructure

and the Dynamics of Soft Matter. *J. Appl. Crystallogr.* **2007**, *40*, s459−s462.
(24) Feigin, L. A.; Svergun, D. I. *Structure Analysis by Small-Angle X-Ray and Neutron Scattering*; Taylor, G. W., Ed.; Springer US: Boston, MA, 1987, DOI: 10.1007/978-1-4757-6624-0.
(25) Putnam, C. D. Guinier Peak Analysis for Visual and Automated Inspection of Small-Angle X-Ray Scattering Data. *J. Appl. Crystallogr.* **2016**, *49*, 1412−1419.
(26) Sreerama, N.; Woody, R. W. Estimation of Protein Secondary Structure from Circular Dichroism Spectra: Comparison of CONTIN, SELCON, and CDSSTR Methods with an Expanded Reference Set. *Anal. Biochem.* **2000**, *287*, 252−260.
(27) Whitmore, L.; Wallace, B. A. DICHROWEB, an Online Server for Protein Secondary Structure Analyses from Circular Dichroism Spectroscopic Data. *Nucleic Acids Res.* **2004**, *32*, W668-73.
(28) Brogan, A. P. S.; Sharma, K. P.; Perriman, A. W.; Mann, S. Isolation of a Highly Reactive β-Sheet-Rich Intermediate of Lysozyme in a Solvent-Free Liquid Phase. *J. Phys. Chem. B* **2013**, *117*, 8400−8407.
(29) Guinier, A.; Fournet, G. *Small-Angle Scattering of X-Rays*; John Wiley & Sons, Ltd: New York, 1955.
(30) Rundlett, K. L.; Armstrong, D. W. Mechanism of Signal Suppression by Anionic Surfactants in Capillary Electrophoresis-Electrospray Ionization Mass Spectrometry. *Anal. Chem.* **1996**, *68*, 3493−3497.
(31) Pérez, B.; Coletta, A.; Pedersen, J. N.; Petersen, S. V.; Periole, X.; Pedersen, J. S.; Sessions, R. B.; Guo, Z.; Perriman, A.; Schiøtt, B. Insight into the Molecular Mechanism behind PEG-Mediated Stabilization of Biofluid Lipases. *Sci. Rep.* **2018**, *8*, 12293.
(32) Zhou, Y.; Jones, N. C.; Pedersen, J. N.; Pérez, B.; Hoffmann, S. V.; Petersen, S. V.; Pedersen, J. S.; Perriman, A.; Kristensen, P.; Gao, R.; Guo, Z. Insight into the Structure and Activity of Surface-Engineered Lipase Biofluids. *ChemBioChem* **2019**, *20*, 1266−1272.
(33) Pedersen, J. S. Form Factors of Block Copolymer Micelles with Spherical, Ellipsoidal and Cylindrical Cores. *J. Appl. Crystallogr.* **2000**, *33*, 637−640.
(34) Morgenstern, J.; Baumann, P.; Brunner, C.; Hubbuch, J. Effect of PEG Molecular Weight and PEGylation Degree on the Physical Stability of PEGylated Lysozyme. *Int. J. Pharm.* **2017**, *519*, 408−417.
(35) da Silva Freitas, D.; Abrahão-Neto, J. Biochemical and Biophysical Characterization of Lysozyme Modified by PEGylation. *Int. J. Pharm.* **2010**, *392*, 111−117.
(36) Malcolm, B. A.; Rosenberg, S.; Corey, M. J.; Allen, J. S.; de Baetselier, A.; Kirsch, J. F. Site-Directed Mutagenesis of the Catalytic Residues Asp-52 and Glu-35 of Chicken Egg White Lysozyme. *Proc. Natl. Acad. Sci. U. S. A.* **1989**, *86*, 133−137.
(37) Armstrong, J. P. K.; Shakur, R.; Horne, J. P.; Dickinson, S. C.; Armstrong, C. T.; Lau, K.; Kadiwala, J.; Lowe, R.; Seddon, A.; Mann, S.; Anderson, J. L. R.; Perriman, A. W.; Hollander, A. P. Artificial Membrane-Binding Proteins Stimulate Oxygenation of Stem Cells during Engineering of Large Cartilage Tissue. *Nat. Commun.* **2015**, *6*, 7405.

https://dx.doi.org/10.1021/acs.biomac.0c01663
Biomacromolecules 2021, 22, 1159−1166